


# Infrared spectra of neutral dimethylamine clusters: An infrared-vacuum ultraviolet spectroscopic and anharmonic vibrational calculation study

Cite as: J. Chem. Phys. **150**, 064317 (2019); <https://doi.org/10.1063/1.5086095>

Submitted: 18 December 2018 . Accepted: 27 January 2019 . Published Online: 14 February 2019

Bingbing Zhang, Qian-Rui Huang, Shukang Jiang, Li-Wei Chen, Po-Jen Hsu, Chong Wang, Ce Hao, Xiangtao Kong, Dongxu Dai, Xueming Yang, Jer-Lai Kuo, and Ling Jiang 



View Online



Export Citation



CrossMark

## ARTICLES YOU MAY BE INTERESTED IN

[Feynman diagram description of 2D-Raman-THz spectroscopy applied to water](#)

The Journal of Chemical Physics **150**, 044202 (2019); <https://doi.org/10.1063/1.5079497>

[Operators in quantum machine learning: Response properties in chemical space](#)

The Journal of Chemical Physics **150**, 064105 (2019); <https://doi.org/10.1063/1.5053562>

[Ab initio studies of the ground and first excited states of the Sr-H<sub>2</sub> and Yb-H<sub>2</sub> complexes](#)

The Journal of Chemical Physics **150**, 064316 (2019); <https://doi.org/10.1063/1.5052653>



# Infrared spectra of neutral dimethylamine clusters: An infrared-vacuum ultraviolet spectroscopic and anharmonic vibrational calculation study

Cite as: J. Chem. Phys. 150, 064317 (2019); doi: 10.1063/1.5086095

Submitted: 18 December 2018 • Accepted: 27 January 2019 •

Published Online: 14 February 2019



Bingbing Zhang,<sup>1,2,3,a)</sup> Qian-Rui Huang,<sup>4,a)</sup> Shukang Jiang,<sup>2,3,5,6</sup> Li-Wei Chen,<sup>4</sup> Po-Jen Hsu,<sup>4</sup> Chong Wang,<sup>2,3</sup> Ce Hao,<sup>1</sup> Xiangtao Kong,<sup>2</sup> Dongxu Dai,<sup>2</sup> Xueming Yang,<sup>2</sup> Jer-Lai Kuo,<sup>4,b)</sup> and Ling Jiang<sup>2,c)</sup>

## AFFILIATIONS

<sup>1</sup>State Key Laboratory of Fine Chemicals, Dalian University of Technology, 2 Linggong Road, Dalian 116024, China

<sup>2</sup>State Key Laboratory of Molecular Reaction Dynamics, Dalian Institute of Chemical Physics, Chinese Academy of Sciences, 457 Zhongshan Road, Dalian 116023, China

<sup>3</sup>University of Chinese Academy of Sciences, 19A Yuquan Road, Beijing 100049, China

<sup>4</sup>Institute of Atomic and Molecular Sciences, Academia Sinica, Taipei 10617, Taiwan

<sup>5</sup>Shanghai Advanced Research Institute, Chinese Academy of Sciences, 99 Haik Road, Shanghai 201210, China

<sup>6</sup>School of Physical Science and Technology, ShanghaiTech University, 319 Yueyang Road, Shanghai 200031, China

<sup>a)</sup> **Contributions:** B. Zhang and Q.-R. Huang contributed equally to this work.

<sup>b)</sup> **E-mail:** jkuo@pub.iam.s.sinica.edu.tw

<sup>c)</sup> **E-mail:** ljiang@dicp.ac.cn

## ABSTRACT

Infrared-vacuum ultraviolet (IR-VUV) spectra of neutral dimethylamine clusters, (DMA)<sub>n</sub> (*n* = 2–5), were measured in the spectral range of 2600–3700 cm<sup>−1</sup>. The experimental IR-VUV spectra show NH stretch modes gradually redshift to 3200–3250 cm<sup>−1</sup> with the increase in the cluster size and complex Fermi Resonance (FR) pattern of the CH<sub>3</sub> group in the 2800–3000 cm<sup>−1</sup> region. *Ab initio* anharmonic vibrational calculations were performed on low-energy conformers of (DMA)<sub>2</sub> and (DMA)<sub>3</sub> to examine vibrational coupling among CH/NH and to understand the Fermi resonance pattern in the observed spectra features. We found that the redshift of NH stretching mode with the size of DMA cluster is moderate, and the overtone of NH bending modes is expected to overlap in frequency with the CH stretching fundamental modes. The FR in CH<sub>3</sub> groups is originated from the strong coupling between CH stretching fundamental and bending overtone within a CH<sub>3</sub> group. Well-resolved experimental spectra also enable us to compare the performance of *ab initio* anharmonic algorithms at different levels.

Published under license by AIP Publishing. <https://doi.org/10.1063/1.5086095>

## I. INTRODUCTION

Vibrational spectroscopy has been one of the most important methods to analyze intramolecular and intermolecular interactions of complexes, providing detailed structural and dynamical information.<sup>1–13</sup> The vibrational features of the C–H, N–H, and O–H stretches in the 3 μm region are often

quite complex because of Fermi Resonance (FR). For instance, the FR interaction between the methylene symmetric C–H stretching mode and the methylene bending mode has been observed in the vibrational spectra of the polymethylene chain.<sup>14</sup> Infrared spectroscopic study of HCO<sub>2</sub><sup>−</sup>, DCO<sub>2</sub><sup>−</sup>, and HCO<sub>2</sub><sup>−</sup>⋯H<sub>2</sub>O revealed that the dominant FR interactions occur between the CH stretch fundamental and both

the in-plane and out-of-plane bending overtones.<sup>15</sup> The CH stretch-bend Fermi couplings have been observed in the CH stretch region for a variety of hydrocarbon systems.<sup>16–19</sup> The  $5n$ -dimensional anharmonic Hamiltonian calculations of neutral  $(\text{NH}_3)_n$  ( $n = 1\text{--}5$ ) clusters indicated that the main players of the FR are the symmetric N–H stretching mode and overtones of the bending mode, and the coupling with overtones of the bending mode becomes more important in the tetramer and the pentamer.<sup>20</sup> Infrared spectra of the  $\text{X}^-\cdot\text{H}_2\text{O}$  ( $\text{X} = \text{Cl}, \text{Br}, \text{I}$ ) complexes evidenced a FR interaction between the ionic hydrogen-bonded O–H stretch and the overtone of the intramolecular bend.<sup>21</sup> Interestingly, the investigation of rare gas-tagged  $\text{H}_3\text{O}^+$  species demonstrated a stronger coupling between the overtones of bending modes and the fundamentals of stretching modes in Ne-tagged  $\text{H}_3\text{O}^+$  than in Ar-tagged  $\text{H}_3\text{O}^+$ .<sup>22–24</sup>

The recent infrared-vacuum ultraviolet (IR-VUV) spectroscopic and *ab initio* anharmonic study of neutral monomethylamine (MMA) dimer indicated that the main origin of the complexity in the spectral range of  $2800\text{--}3000\text{ cm}^{-1}$  is caused by FR between the stretching and the bending overtones of the  $\text{CH}_3$  group.<sup>25,26</sup> Dimethylamine (DMA) is a molecule with two nonpolar  $\text{CH}_3$  groups and one polar NH group, which affords a model system for studying the coupling among different  $\text{CH}_3$  groups and NH groups. Microwave spectroscopic studies of DMA dimer and trimer suggested that  $(\text{DMA})_2$  has a structure of  $\text{C}_s$  symmetry and  $(\text{DMA})_3$  consists of a cyclic structure.<sup>27,28</sup> IR spectroscopic measurements of neutral dimethylamine clusters remain elusive so far. Herein, we report the IR spectra of neutral dimethylamine clusters,  $(\text{DMA})_n$  ( $n = 2\text{--}5$ ), in the spectral range of  $2600\text{--}3700\text{ cm}^{-1}$ . The experimental spectra are analyzed with the help of calculated spectra from *ab initio* anharmonic algorithms.

## II. EXPERIMENTAL METHOD

Experiments were carried out on a previously described Dalian IR-VUV apparatus.<sup>26</sup> The VUV light at 118 nm used in this study was generated by third harmonic generation (355 nm) of a Nd:YAG laser (Nimma-600) via a Xe/Ar gas mixture at 1:10 relative concentration for 200 Torr total pressure. A beam of neutral complexes was generated from supersonic expansions of 5% DMA seeded in He using a pulsed valve (General Valve, Series 9) at 5 atm backing pressure and passed through a 4 mm diameter skimmer and an aperture with 3 mm opening. The cations were produced from the 118 nm one-photon ionization process in the center of the extraction region of a reflectron time-of-flight (TOF) mass spectrometer, and the signal intensity of the particular mass channel was monitored. Here, the tunable IR light pulse was introduced at about 55 ns prior to the VUV laser pulse in a crossed manner. When the resonant vibrational transition with the IR light caused vibrational predissociation, the dissociation induced depopulation of the neutral cluster. The depopulation can be monitored as a reduction of the ion signal intensity in the cluster mass channel. An IR spectrum of the size-selected neutral species was obtained as a depletion spectrum of the monitored ion signal intensity by scanning the IR wavelength. The

VUV laser was operated at 20 Hz, and IR laser was operated at 10 Hz. IR spectra were recorded in the difference mode of operation.

The tunable IR laser beam was generated by using a potassium titanyl phosphate (KTP)/Potassium Titanyl Arsenate (KTA) optical parametric oscillator/amplifier system (OPO/OPA, LaserVision)<sup>29</sup> pumped by an injection-seeded Nd:YAG laser (Continuum Surelite EX). This system is tunable from  $700$  to  $7000\text{ cm}^{-1}$  with a linewidth of  $1\text{ cm}^{-1}$ . The wavelength of the OPO laser output was calibrated using a commercial wavelength meter (Bristol, 821 Pulse Laser Wavelength Meter). The IR spectrum was obtained by converting from the measured relative depletion of the mass spectrometric ion signal  $(I(v)/I_0)$  upon irradiation with IR light to relative absorption cross sections  $\sigma(v)$  using  $\sigma(v) = -\ln[I(v)/I_0]/P(v)$ . The normalization with the IR laser pulse energy  $P(v)$  accounted for its variations over the tuning range.

## III. COMPUTATIONAL METHODS

### A. Structures of DMA clusters

The structures of neutral  $(\text{NH}_3)_n$  and  $(\text{MMA})_n$  have been searched previously, and the stable structures of small clusters ( $n = 3$  and  $4$ ) form the hydrogen bond in a cyclic form.<sup>20,25,30</sup> Based on the structures of  $(\text{MMA})_n$ , we generated different conformers of  $(\text{DMA})_n$  by replacing the free (non-HB) hydrogen atom on each MMA by a  $\text{CH}_3$  group. Due to the additional  $\text{CH}_3$  group in DMA, the role of dispersion can be more significant. Thus, we have also carried out random search on DMA clusters using B3LYP hybrid functional augmented with a dispersion correction (DFTB-D3). These initial structures were first checked with their structural similarity by following the procedure we developed earlier.<sup>31</sup> Only distinct conformers underwent geometry optimizations (first by B3LYP/6-31+G\* and then verified by MP2/aug-cc-pVDZ). Structures of low-energy isomers are shown in Fig. 1 with their relative energetics. We found three conformers for the DMA dimer. Conformer 2a and 2b are hydrogen-bonded (H-Bonded) structures with a relative energy of  $1.6\text{ kJ/mol}$ . In the most stable conformer of trimer (3a), all DMA molecules are single-donor-single-acceptors. Conformer 3b has two hydrogen bonds, and thus, every DMA molecule has a different coordination number (one single-donor, one single-donor-single-acceptor, and one single-acceptor). In addition to the H-Bonded structures shown in Fig. 1, we found several non-HB conformers. The structure shown in 2c is a non-HB conformer, and it has a relative higher energy of  $5.9\text{ kJ/mol}$ .

### B. *Ab initio* anharmonic method—Quartic potential

One of our anharmonic algorithms based on quartic potential (QP) and direct diagonalization of vibrational Hamiltonian has recently been applied to study Fermi resonance in ammonia and MMA clusters.<sup>20,25</sup> The details of the methodology can be found in the previous publications; thus, we will only include a brief summary here. In our treatment, the anharmonic vibrational Hamiltonian included all the cubic and part of the quartic terms in the potential energy operator,

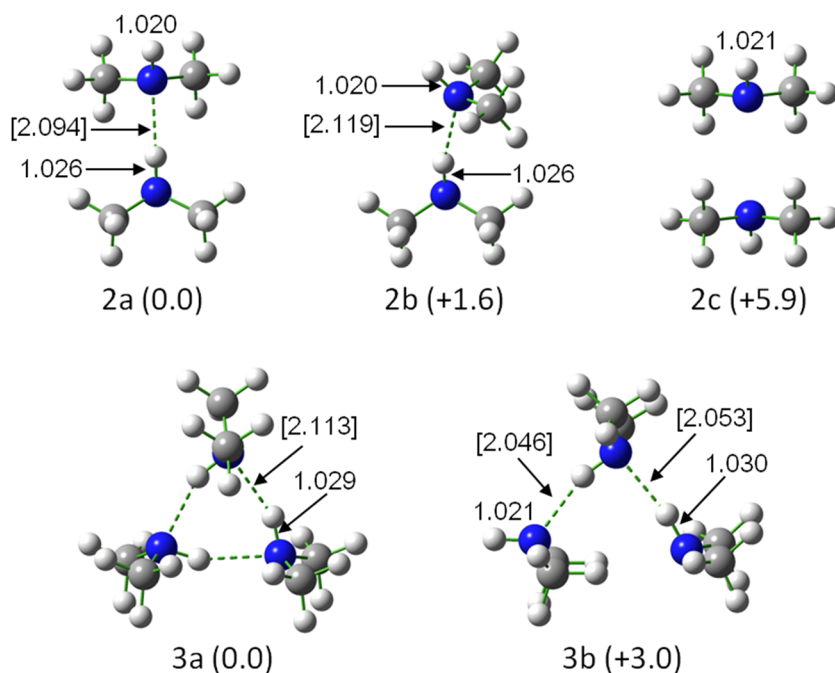


**FIG. 1.** Optimized structures of neutral  $(\text{DMA})_n$  ( $n = 2$  and  $3$ ) clusters. MP2/aug-cc-pVDZ relative energies (in kJ/mol) are listed inside round brackets. The N–H and N–H...N (inside square brackets) bond distances are given in Å.

$$V = \sum_i \frac{1}{2} f_{ii} q_i^2 + \sum_{i,j,k} \frac{1}{6} f_{ijk} q_i q_j q_k + \sum_{i,j,k,l} \frac{1}{24} f_{ijkl} q_i q_j q_k q_l,$$

where  $q_i$  is a mass-weighted coordinate along the  $i$ th normal mode. To analyze the coupling among normal modes in different functional groups, we used a normal mode localized in either a molecule or a functional group to expand the vibrational Hamiltonian. Second derivatives with MP2/aug-cc-pVDZ were computed analytically with the Gaussian 09 program.<sup>32</sup> The third and fourth derivatives were then evaluated by numerical finite difference methods from analytical second derivatives. Following this procedure, only the semi-diagonal (up to three body or three different-modes) of the quartic terms was included. This QP form of the *ab initio* anharmonic Hamiltonian was commonly used in many anharmonic analyses.<sup>33,34</sup> Instead of using perturbation theory, we cast the Hamiltonian matrix using direct product of harmonic oscillator wavefunctions as basis, and direct diagonalization was used to solve eigen-value problems.

For a given conformer of  $(\text{DMA})_n$ , we considered up to  $14n$  degrees of freedom (DOF): including  $n$  NH stretch,  $6n$  CH stretch,  $n$  NH bend,  $4n$  CH<sub>3</sub> bending, and  $2n$  CH<sub>3</sub> umbrella modes. Construction of the vibrational Hamiltonian for a DMA cluster is much more expensive than their counterparts in ammonia and MMA clusters. The number of DOF in a DMA cluster is much larger than the other two clusters; for example, the CH stretch and CH bend in a DMA trimer need 36 DOF, which makes the basis size to  $\sim 1 \times 10^6$ ; meanwhile, the computing time to evaluate one Hessian at MP2/aug-cc-pVDZ of DMA dimer is comparable to that of an ammonia pentamer

and a MMA trimer. Therefore, we have examined up to the DMA trimer with our anharmonic algorithm based on quartic potential.

### C. *Ab initio* anharmonic method—Discrete variable representation

In the above-mentioned *ab initio* anharmonic algorithm, the potential energy surface (PES) term was truncated at the fourth order. To access the error caused by neglecting the higher order terms in QP, we used discrete variable representation (DVR) to compute the vibrational coupling among the six vibrational modes of a CH<sub>3</sub> group in the DMA monomer. Our DVR implementation has been detailed in a few recent publications.<sup>23,24</sup> Since only PES is needed in DVR and there is no need to have analytical Hessian implemented in quantum chemical packages, we can use higher level of electronic structure methods [such as coupled-cluster single double (CCSD)] to test the convergence on the level of quantum chemistry method. The main drawback of DVR is the unfavorable scaling with respect to the number of DOF and grid points. Due to the limitation of the matrix size in DVR, we examined the coupling among the six DOFs in a CH<sub>3</sub> group, and we used 5 grid points for all modes; thus, we need  $5^6 = 15\,625$  grid points to build a full 6D PES. Scanning the whole 6D PES with CCSD is computationally expensive; hence, we truncated the PES to 5-mode representation (MR),<sup>22</sup> and we utilized the “mixed-level approach,” which computed the different  $n$ -mode coupling with the different level of theory. We calculated all 1MR and 2MR couplings with CCSD/aug-cc-pVDZ, and all 3MR–5MR couplings were calculated with MP2/aug-cc-pVDZ.

This method allows us to obtain the same accuracy with the CCSD method with a fraction of the computational cost.

## IV. RESULTS AND DISCUSSION

### A. Experimental results

Figure 2 shows the mass spectra of DMA clusters generated by the 118 nm single-photon ionization under different experimental conditions. Two series of DMA clusters are observed, one unprotonated  $(\text{DMA})_n^+$  and the other protonated  $\text{H}^+(\text{DMA})_n$ . With a proton affinity  $\sim 930$  kJ/mol,<sup>35</sup> DMA could easily pick up a proton, which is similar to ammonia,<sup>36</sup> monomethylamine,<sup>26</sup> and methanol.<sup>37</sup>

During the preparation for DMA clusters, various experimental conditions (i.e., concentration of DMA/helium mixture, type of nozzle, intensity of main spring and buffer spring of General Valve, and stagnation pressure) were optimized to maximize the signal of the cluster with interest and minimize the contribution from larger clusters. For instance, it can be seen from Fig. 2 that under experimental condition (i), the  $(\text{DMA})_2^+$  cluster is clearly observed while the signal of  $(\text{DMA})_3^+$  is negligible. Infrared spectra of neutral  $(\text{DMA})_2$  were recorded by monitoring the depletion for the intensity of the  $(\text{DMA})_2^+$  mass channel under experimental condition (i). IR laser power dependence was performed to check the saturation effect, as shown in Fig. 3. Bands A–D were observed with various IR laser powers conditions a–c. By contrast, the asterisk-labeled band at  $2941\text{ cm}^{-1}$  was observed with higher IR laser power at condition (a) but absent with lower IR laser powers at conditions (b) and (c). As demonstrated before, for the first overtone of the antisymmetric O–H stretching in the infrared photodissociation spectra of  $[\text{MgNO}_3(\text{H}_2\text{O})_n]^+$  ( $n = 1\text{--}3$ ),<sup>38</sup> the intensity of a higher order excitation is more sensitive to the IR laser power. This asterisk-labeled band fits

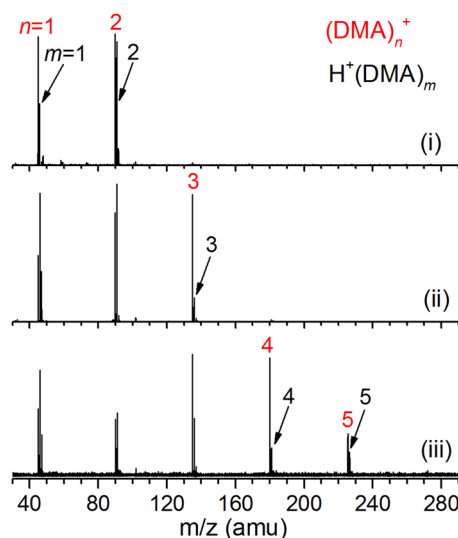


FIG. 2. Mass spectra of dimethylamine (DMA) clusters generated by 118 nm single-photon ionization.

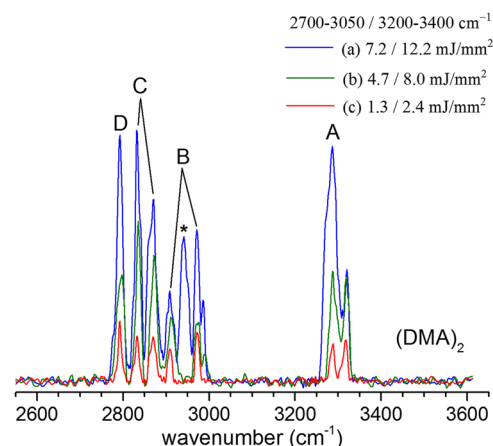


FIG. 3. IR laser power dependence for infrared spectra of neutral  $(\text{DMA})_2$ .

such a behavior very well, with its disappearance at low IR laser power, and is assigned to an overtone or combination band.

Analogously, IR spectra of neutral  $(\text{DMA})_3$  and  $(\text{DMA})_n$  ( $n = 4$  and  $5$ ) were measured under the experimental conditions (ii) and (iii) shown in Fig. 2, respectively. IR laser power dependence of  $(\text{DMA})_n$  ( $n = 3\text{--}5$ ) is illustrated in Figs. S1–S3, respectively. The best resolution for IR spectra of  $(\text{DMA})_n$  ( $n = 2\text{--}5$ ) was achieved at a low IR laser power of  $\sim 2$  mJ/mm<sup>2</sup>, which is shown in Fig. 4. It can be seen from Fig. 4 that the IR spectrum for each individual cluster is different from each other, indicating negligible contribution from larger clusters. Experimental frequencies of  $(\text{DMA})_n$  ( $n = 2\text{--}5$ ) are summarized in Table I. Band A appears at  $3288$  and  $3318\text{ cm}^{-1}$  in the

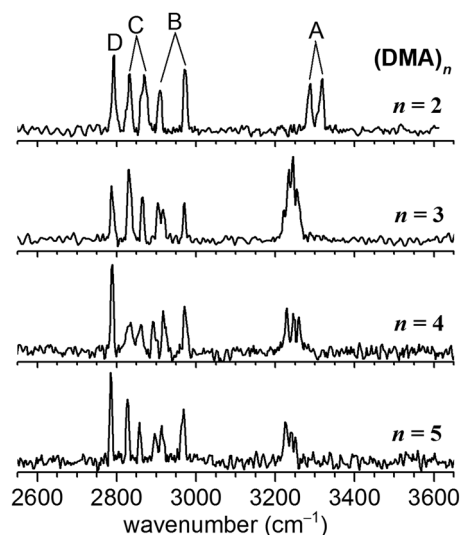


FIG. 4. Experimental IR spectra of neutral  $(\text{DMA})_n$  ( $n = 2\text{--}5$ ) clusters measured at the experimental conditions (i)–(iii) shown in Fig. 2 and condition (c) shown in Fig. 3 and Figs. S1–S3.



**TABLE I.** Experimental band positions (in  $\text{cm}^{-1}$ ) and band assignments for neutral  $(\text{DMA})_n$  ( $n = 2-5$ ) clusters.

Label	$n = 2$	$n = 3$	$n = 4$	$n = 5$	Assignment
A	3318	3254	3259	3250	Hydrogen-bonded N-H stretch
	3288	3244	3245	3240	
		3234	3229	3224	
		3222			
B	2971	2971	2971	2969	Antisymmetric C-H stretch ( $\nu_2$ , $\nu_{11}$ )
	2909	2917	2917	2913	
		2903	2891	2895	
C	2869	2865	2861	2857	The coupling between symmetric C-H stretch ( $\nu_3$ ) and C-H bending overtones ( $2\nu_6/\nu_6 + \nu_5/2\nu_5/2\nu_{12}$ )
	2833	2831	2830	2827	
D	2793	2787	2786	2785	The coupling between symmetric C-H stretch ( $\nu_3$ ) and C-H bending overtones ( $2\nu_6/\nu_6 + \nu_5/2\nu_5/2\nu_{12}$ )

$n = 2$  cluster, shows multiple splitting at 3222, 3234, 3244, and  $3254 \text{ cm}^{-1}$  at  $n = 3$ , and then redshifts slightly by  $5-10 \text{ cm}^{-1}$  at  $n = 4$  and  $5$ . Bands B-D show small redshifts by  $\sim 10 \text{ cm}^{-1}$  from  $n = 2$  to  $n = 5$ . Based on the previous studies of neutral MMA clusters,<sup>25,26</sup> band A can be assigned to the hydrogen-bonded N-H stretching. The splitting of band A in the IR spectrum of DMA dimer could be stemmed from the structural transformation and the fluctuation of hydrogen bond distance as previously reported for the MMA dimer.<sup>26</sup> The complex features observed in the  $2700-3100 \text{ cm}^{-1}$  region (bands B-D) should be due to the C-H stretching. The recent *ab initio* anharmonic analysis of neutral  $(\text{MMA})_2$  cluster indicated that the main origin of the complexity in the  $2700-3100 \text{ cm}^{-1}$  region was caused by Fermi resonance (FR) between the stretching and bending overtones of the  $\text{CH}_3$  group.<sup>25</sup> Herein, both harmonic and *ab initio* anharmonic calculations were performed on the DMA clusters to explore vibrational coupling of C-H/N-H and to understand the observed spectral features.

## B. Harmonic spectra

The comparison of experimental IR spectra to harmonic spectra of DMA dimer and trimer calculated at the MP2/aug-cc-pVDZ level is given in Figs. 5 and 6, respectively. Among the three conformers of DMA dimer, conformers 2a and 2b have very similar spectra with a hydrogen-bonded N-H stretching mode. For DMA trimer, conformer 3a has three-fold symmetry, so there is a doubly degenerated set of asymmetric NH stretch modes. In the calculated harmonic spectrum of conformer 3b, the two hydrogen-bonded N-H stretching modes have slightly different frequencies.

The bright states in the  $2800-3000 \text{ cm}^{-1}$  region are the C-H stretching modes in the  $\text{CH}_3$  groups. We follow the same naming of vibrational modes of the  $\text{CH}_3$  group in DMA as the previous study of FR in MMA:  $\text{CH}_3^a$  d-str ( $\nu_{11}$ ),  $\text{CH}_3^a$  d-str ( $\nu_2$ ),  $\text{CH}_3^a$  s-str ( $\nu_3$ ).<sup>39</sup> In conformer 2c, all  $\text{CH}_3$  groups are identical; thus, each type of CH stretching mode has four-fold degeneracy. In conformers 2a and 2b, CH stretching modes on donor DMA are systematically lower than their counterparts on the acceptor DMA. While the relative energy of 2a and 2b is

$1.6 \text{ kJ/mol}$ , the difference in their spectral pattern is minimal. The CH stretching modes in conformers 3a and 3b are consistent with their hydrogen bonding coordination. In conformer 3a, all DMA are single-donor-and-single acceptors, so their CH stretching modes are simple. In conformer 3b, every DMA is different; thus, the frequency of their CH stretching modes differs slightly.

## C. Anharmonic spectra

From the harmonic analysis, we can see that the NH group of non-HB conformers makes very minor contribution to the spectral pattern above  $3200 \text{ cm}^{-1}$  and their spectral patterns originating from the  $\text{CH}_3$  group (in the  $2800-3000 \text{ cm}^{-1}$  region) are very similar to the monomer. In the following, we

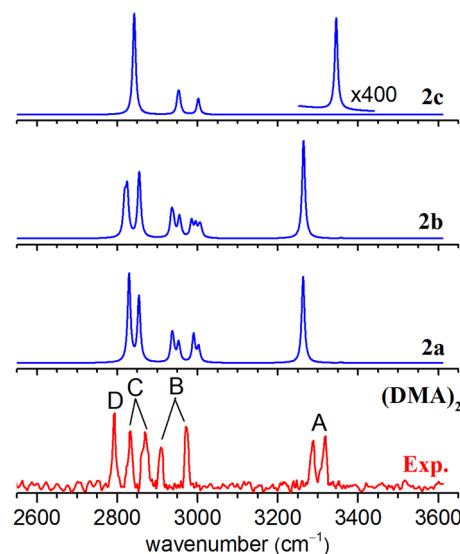


**FIG. 5.** Comparison of experimental IR spectrum with MP2/aug-cc-pVDZ harmonic IR spectra for  $(\text{DMA})_2$ . Harmonic frequencies were scaled by 0.950, and the resulting stick spectra were convoluted by a Gaussian line shape function with a width of  $9 \text{ cm}^{-1}$  (fwhm).

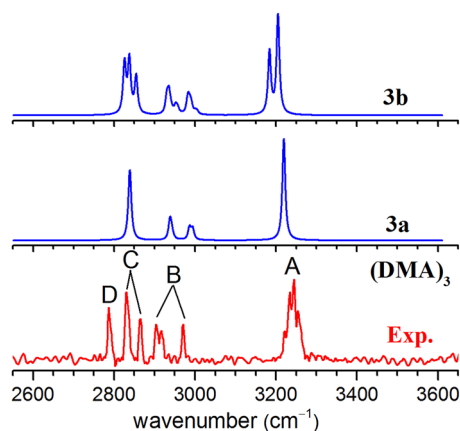


**FIG. 6.** Comparison of experimental IR spectrum with MP2/aug-cc-pVDZ harmonic IR spectra for  $(\text{DMA})_3$ . Harmonic frequencies were scaled by 0.950, and the resulting stick spectra were convoluted by a Gaussian line shape function with a width of  $9\text{ cm}^{-1}$  (fwhm).

will focus on the analysis of anharmonic spectra of the HB conformers. Experimental spectra of DMA dimer and trimer are compared with anharmonic spectra of the HB conformers in Fig. 7.

### 1. Weak coupling among vibrational modes localized on different functional groups

In a previous study, we found the vibrational coupling between  $\text{CH}_3$  and  $\text{NH}_2$  groups in a MMA molecule or small cluster is negligible.<sup>25</sup> In a DMA molecule, there are three functional groups (two  $\text{CH}_3$  groups and one  $\text{NH}$  group). We have also performed detailed analysis to confirm that vibrational coupling among these groups is small by comparing anharmonic spectra of DMA monomer calculated with different low-dimensional anharmonic Hamiltonians. For DMA dimer, we found this approximation remains well justified in all three conformers. The details can be found in Fig. S4.

### 2. Fermi resonance in NH group

Each DMA has only one N-H stretching and one N-H bending mode; thus, FR in the NH group of DMA is simpler than that in MMA. The main difference between the amine groups in MMA and DMA clusters is that the frequency of N-H bending in DMA is lower than that of the  $\text{NH}_2$  bending in MMA ( $\sim 1600\text{ cm}^{-1}$  in MMA and  $\sim 1500\text{ cm}^{-1}$  in DMA). In Fig. 7, the overtone of N-H bending in DMA is found to be located at slight above  $3000\text{ cm}^{-1}$ .

The spectral feature of NH groups by two H-Bonded dimers (2a and 2b) are dominated by the donor DMA. The frequency of H-Bonded N-H stretching in donor DMA is  $\sim 3300\text{ cm}^{-1}$ . Even though the mis-match in the frequency (between overtone of bending mode and fundamental of stretching modes) is more than  $250\text{ cm}^{-1}$ , overtone of bending manages to borrow some intensity from N-H stretching. This is consistent with the notion that the FR coupling strength is

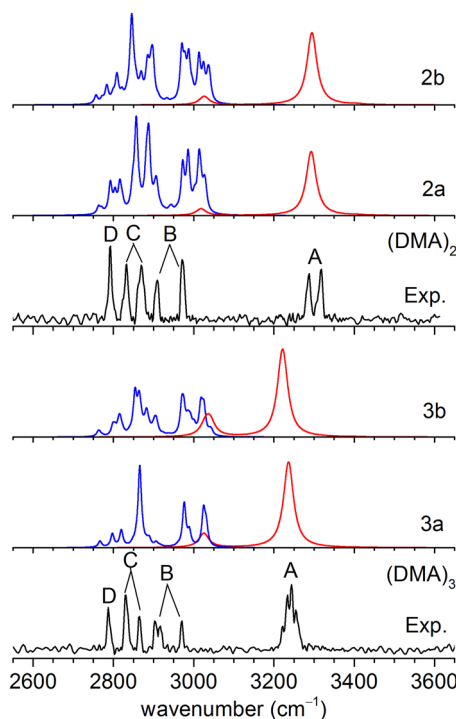


**FIG. 7.** Comparison of experimental IR spectra of DMA clusters to anharmonic spectra of the isomers shown in Fig. 1. Vibrational spectra calculated with explicit cross coupling for the stretching modes of  $\text{CH}_3$  are shown in blue and those for the  $\text{NH}$  group in red. For better comparison to experiments, the calculated spectra are broadened with a homogeneous width of 15 and  $5\text{ cm}^{-1}$  for the  $\text{NH}$  and  $\text{CH}$  modes, respectively.

expected to be similar to MMA ( $\sim 50\text{ cm}^{-1}$ ). Since the binding energies of conformers 2a and 2b are similar, their anharmonic spectra are almost identical. In the conformers of 3a and 3b, the frequencies of N-H stretch decrease to  $\sim 3200\text{ cm}^{-1}$  and the reduction in the energy mis-match (less than  $200\text{ cm}^{-1}$ ) enhances the intensity of the overtone states, and the peaks at  $\sim 3000\text{ cm}^{-1}$  become more obvious.

Due to computational cost, our anharmonic calculations are limited to the DMA trimer. For larger clusters, we expect the frequency of N-H stretching modes will be slightly reduced (due to cooperative effect) and thus the intensity of the overtone states will be further strengthened. One should note that the frequency of NH bending overtone appears in the similar region of the fundamental of C-H stretching modes.

### 3. Anharmonic spectra of the $\text{CH}_3$ groups calculated with quartic potential

Anharmonic spectra of the  $\text{CH}_3$  groups on different conformers of DMA clusters calculated with QP are shown in Fig. 8. To analyze the Fermi resonance between the fundamental C-H stretching and C-H bending overtones, we first performed 2 separate QP calculations on (1) all C-H stretching modes and (2) all C-H bending modes; the QP Hamiltonians

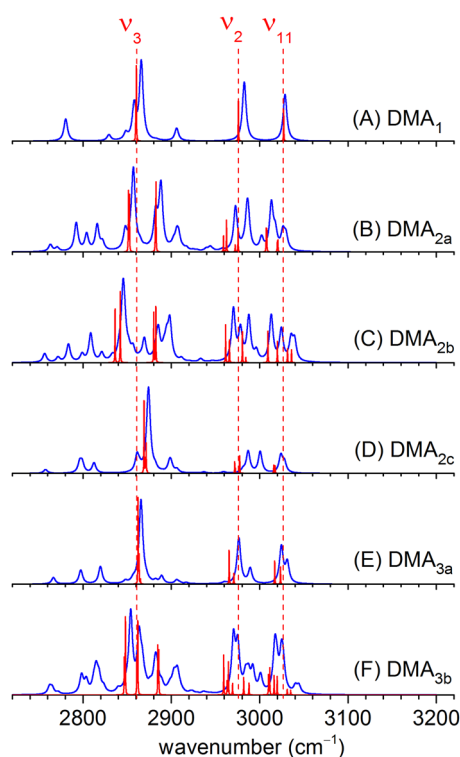


**FIG. 8.** Anharmonic spectra of the CH<sub>3</sub> groups on different conformers of DMA clusters calculated with QP. The red dashed lines are drawn for eye-guiding purposes to connect the same types of C–H stretching modes in these DMA clusters.

of these two systems are labeled  $H_s$  and  $H_b$ , and the resulting eigenvectors are labeled  $|\psi_s^{n_s}\rangle$  and  $|\psi_b^{n_b}\rangle$ , in which  $n_s$  and  $n_b$  act as the quantum numbers. Subsequently, the QP Hamiltonian for the whole CH<sub>3</sub> groups,  $H_{CH_3}$ , can be partitioned as follow:

$$H_{CH_3} = H_s + H_b + V_{sb}$$

in which  $V_{sb}$  is the coupling between stretching modes and bending modes. The Hamiltonian can thus be recast using the direct product wavefunction  $|n_s, n_b\rangle$  as the basis, which is defined as follow:

$$|n_s, n_b\rangle = |\psi_s^{n_s}\rangle \times |\psi_b^{n_b}\rangle.$$

In this context, the fundamental C–H stretching is labeled  $|1, 0\rangle$ , and the C–H bending overtone is  $|0, 2\rangle$ . The red lines in Fig. 8 show the fundamental stretchings without the influence from bending overtones; the frequencies can be obtained as the diagonal terms  $\langle 1, 0 | H_{CH_3} | 1, 0 \rangle$ ; meanwhile, the intensity can be estimated by evaluating the transition dipole moment  $\langle 0 | H_{CH_3} | 1, 0 \rangle$ , in which the initial state  $\langle 0 |$  is the ground state of  $H_{CH_3}$ . The off-diagonal terms  $\langle 0, 2 | H_{CH_3} | 1, 0 \rangle$  can be viewed as the coupling between stretching and bending overtone, which is the main cause of Fermi resonance.

It can be seen from Fig. 8 that the position of three kinds of C–H stretching modes is well separated and is not sensitive to the size of the cluster. The peak position of  $\nu_{11}$  and  $\nu_2$  in  $(DMA)_n$  ( $n = 1-3$ ) is very similar. The peak position of  $\nu_3$  in DMA clusters is slightly redshifted by 40 cm<sup>-1</sup> from  $n = 1$  to  $n = 3$ . In DMA monomer, because of the weak coupling between two CH<sub>3</sub> groups, the  $\nu_{11}$ ,  $\nu_2$ , and  $\nu_3$  modes on both CH<sub>3</sub> groups are almost degenerated. Spectra of conformers 2a and 2b are shown in Figs. 8(b) and 8(c); frequencies of the stretching modes on the donor DMA are lower than those of the acceptor DMA by ~10 cm<sup>-1</sup>. Therefore, stretching modes in all three manifolds split into doublets (one set originates from donor DMA and the other set from acceptor DMA). Based on the same notion, it is not surprising to see the stretching modes of conformer 2c are almost degenerated and well separated into three distinct manifolds. In conformer 3a, all DMA molecules are identical (single-donor-single-acceptor); thus the stretching modes on each DMA are again very simple. In conformer 3b, every DMA molecule has a different coordination number (one single-donor, one single-acceptor, and one single-donor-single-acceptor); thus, we can see from Fig. 8(f) that the  $\nu_3$  modes are splitted into three groups.

To help analyzing FR, we follow the naming of vibrational modes of the CH<sub>3</sub> group on MMA and name the two bending modes to be  $\nu_{12}$  and  $\nu_5$ , and the umbrella mode is referred to as  $\nu_6$ . If we turn on cross coupling between bending overtones and stretching fundamental, more complex spectra (shown in blue lines) of these conformers as a result of FR can be seen. The Fermi resonance in the CH<sub>3</sub> group of DMA monomer is very similar to that of MMA monomer. By analyzing the matrix elements between overtones of bending modes ( $\nu_6$ ,  $\nu_5$ ,  $\nu_{12}$ ) and fundamental of stretching modes ( $\nu_3$ ,  $\nu_2$ ,  $\nu_{11}$ ) of CH<sub>3</sub> group, two points can be made. First,  $\nu_6 + \nu_{12}$  and  $\nu_5 + \nu_{12}$  couple only to  $\nu_{11}$ . The weaker coupling and a frequency detuning of more than 100 cm<sup>-1</sup> both  $\nu_6 + \nu_{12}$  and  $\nu_5 + \nu_{12}$  (~2900 cm<sup>-1</sup>) could not borrow significant intensity to make them visible. So, the high-frequency is assigned to  $\nu_{11}$ . Second,  $2\nu_6$ ,  $\nu_6 + \nu_5$ ,  $2\nu_5$  and  $2\nu_{12}$  couple only to  $\nu_3$  and  $\nu_2$ . Because of the better energy matching and stronger coupling with overtone states,  $\nu_2$  plays a minor role in the FR. So, the second highest frequency is assigned to  $\nu_2$ . The rest of the spectral features originate from the coupling between  $\nu_3$  and  $2\nu_6/\nu_6 + \nu_5/2\nu_5/2\nu_{12}$ .

#### 4. Benchmarking anharmonic algorithms against experimental data

The weak coupling among different CH<sub>3</sub> groups enables us to use one of the CH<sub>3</sub> groups on the DMA monomer as an example to benchmark the accuracy of quartic potential at MP2/aug-cc-pVDZ in describing the vibrational spectra of CH<sub>3</sub> groups in DMA. The spectrum of DMA monomer with quartic potential (at MP2/aug-cc-pVDZ) is shown in Fig. 9(a). The spectra calculated with numerical PES with DVR methods (at MP2/aug-cc-pVDZ and CCSD/aug-cc-pVDZ) are shown in Figs. 9(b) and 9(c), respectively. Since the spectral features of CH<sub>3</sub> in DMA clusters show little size dependence, the experimental IR spectrum of DMA trimer is shown in Fig. 9



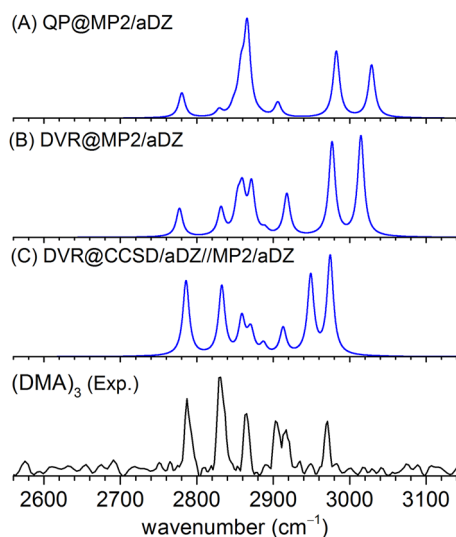


**FIG. 9.** Accuracy of quartic potential in describing the vibrational spectra of  $\text{CH}_3$  groups in the DMA monomer is benchmarked against numerical PES using DVR. Experimental data of DMA trimer reported are shown at the bottom for comparison.

for comparison. It can be found that the agreement between anharmonic calculations and experimental data is gradually improved as the level of theory increases. This benchmark comparison points out the convergence of anharmonic theories to experimental spectra is slow. A higher level of electronic structure theories (both high-order terms of PES and quantum chemistry level beyond MP2) might be required to accurately capture the intensity borrowing.

## V. CONCLUSION

Vibrational spectra of neutral dimethylamine clusters  $(\text{DMA})_n$  ( $n = 2-5$ ) have been examined by IR-VUV spectroscopy combined with *ab initio* anharmonic calculations. Experimental spectra reveal well resolved patterns belong to the NH (above  $3200\text{ cm}^{-1}$ ) and  $\text{CH}_3$  ( $2800-3000\text{ cm}^{-1}$ ) groups. For the NH stretching modes, we observed a moderate redshift as the DMA cluster size increases, but there is no obvious sign of FR in this region. Our anharmonic calculations indicate that the overtone of NH bending would appear in the frequency range that overlaps with the CH stretching modes and thus can be further probed with clusters of  $(\text{CD}_3)_2\text{NH}$ . The complex FR pattern in  $\text{CH}_3$  groups is originated from the strong coupling between CH stretching and bending overtone within a  $\text{CH}_3$  group; therefore, there is little dependence on the cluster size.

## SUPPLEMENTARY MATERIAL

See [supplementary material](#) for the IR laser power dependence for infrared spectra of neutral  $(\text{DMA})_n$  ( $n = 3-5$ ) (Figs. S1-S3) and anharmonic vibrational spectra of a DMA monomer to confirm the weak coupling among the three functional groups (two  $\text{CH}_3$  groups and one NH group) of a DMA (Fig. S4).

## ACKNOWLEDGMENTS

This work was supported by the National Natural Science Foundation of China (Grant Nos. 21673231, 21327901, and 21688102), the Dalian Institute of Chemical Physics (No. DICP DCLS201702), and the Strategic Priority Research Program (Grant No. XDB17000000) of the Chinese Academy of Science. Q.-R.H., P.-J.H., L.-W.C., and J.-L.K. were supported by the Ministry of Science and Technology of Taiwan (Nos. MOST-106-2811-M-001-051 and MOST-107-2628-M-001-002-MY4) and Academia Sinica. Computational resources were supported in part by the National Center for High Performance Computing.

## REFERENCES

- <sup>1</sup>T. S. Zwier, *Annu. Rev. Phys. Chem.* **47**, 205–241 (1996).
- <sup>2</sup>J. J. Scherer, J. B. Paul, A. Okeefe, and R. J. Saykally, *Chem. Rev.* **97**, 25–51 (1997).
- <sup>3</sup>E. J. Bieske and O. Dopfer, *Chem. Rev.* **100**, 3963–3998 (2000).
- <sup>4</sup>U. Buck and F. Huisken, *Chem. Rev.* **100**, 3863–3890 (2000).
- <sup>5</sup>M. A. Duncan, *Int. Rev. Phys. Chem.* **22**, 407–435 (2003).
- <sup>6</sup>W. H. Robertson and M. A. Johnson, *Annu. Rev. Phys. Chem.* **54**, 173–213 (2003).
- <sup>7</sup>J. M. Lisy, *J. Chem. Phys.* **125**, 132302 (2006).
- <sup>8</sup>Y. Matsuda, N. Mikami, and A. Fujii, *Phys. Chem. Chem. Phys.* **11**, 1279–1290 (2009).
- <sup>9</sup>T. R. Rizzo, J. A. Stearns, and O. V. Boyarkin, *Int. Rev. Phys. Chem.* **28**, 481–515 (2009).
- <sup>10</sup>A. Fujii and K. Mizuse, *Int. Rev. Phys. Chem.* **32**, 266–307 (2013).
- <sup>11</sup>N. Heine and K. R. Asmis, *Int. Rev. Phys. Chem.* **34**, 1–34 (2015).
- <sup>12</sup>O. Dopfer and M. Fujii, *Chem. Rev.* **116**, 5432–5463 (2016).
- <sup>13</sup>K. Schwing and M. Gerhards, *Int. Rev. Phys. Chem.* **35**, 569–677 (2016).
- <sup>14</sup>R. G. Snyder, S. L. Hsu, and S. Krimm, *Spectrochim. Acta, Part A* **34**, 395–406 (1978).
- <sup>15</sup>H. K. Gerardi, A. F. DeBlase, X. Su, K. D. Jordan, A. B. McCoy, and M. A. Johnson, *J. Phys. Chem. Lett.* **2**, 2437–2441 (2011).
- <sup>16</sup>E. G. Buchanan, J. C. Dean, T. S. Zwier, and E. L. Sibert III, *J. Chem. Phys.* **138**, 064308 (2013).
- <sup>17</sup>E. L. Sibert III, N. M. Kidwell, and T. S. Zwier, *J. Phys. Chem. B* **118**, 8236–8245 (2014).
- <sup>18</sup>E. L. Sibert III, D. P. Tabor, N. M. Kidwell, J. C. Dean, and T. S. Zwier, *J. Phys. Chem. A* **118**, 11272–11281 (2014).
- <sup>19</sup>D. P. Tabor, R. Kusaka, P. S. Walsh, E. L. Sibert III, and T. S. Zwier, *J. Phys. Chem. Lett.* **6**, 1989–1995 (2015).
- <sup>20</sup>K.-L. Ho, L.-Y. Lee, M. Katada, A. Fujii, and J.-L. Kuo, *Phys. Chem. Chem. Phys.* **18**, 30498–30506 (2016).
- <sup>21</sup>P. Ayotte, G. H. Weddle, J. Kim, and M. A. Johnson, *J. Am. Chem. Soc.* **120**, 12361–12362 (1998).
- <sup>22</sup>Q.-R. Huang, T. Nishigori, M. Katada, A. Fujii, and J.-L. Kuo, *Phys. Chem. Chem. Phys.* **20**, 13836–13844 (2018).
- <sup>23</sup>J. A. Tan, J.-W. Li, C.-C. Chiu, H.-Y. Liao, H. T. Huynh, and J.-L. Kuo, *Phys. Chem. Chem. Phys.* **18**, 30721–30732 (2016).
- <sup>24</sup>J.-W. Li, M. Morita, K. Takahashi, and J.-L. Kuo, *J. Phys. Chem. A* **119**, 10887–10892 (2015).
- <sup>25</sup>Q.-R. Huang, Y.-C. Li, K.-L. Ho, and J.-L. Kuo, *Phys. Chem. Chem. Phys.* **20**, 7653–7660 (2018).
- <sup>26</sup>B. Zhang, X. Kong, S. Jiang, Z. Zhao, D. Yang, H. Xie, C. Hao, D. Dai, X. Yang, Z.-F. Liu, and L. Jiang, *J. Phys. Chem. A* **121**, 7176–7182 (2017).
- <sup>27</sup>J. A. Odutola, R. Viswanathan, and T. R. Dyke, *J. Am. Chem. Soc.* **101**, 4787–4792 (1979).
- <sup>28</sup>M. J. Tubergen and R. L. Kuczkowski, *J. Chem. Phys.* **100**, 3377–3383 (1994).
- <sup>29</sup>W. R. Bosenberg and D. R. Guyer, *J. Opt. Soc. Am. B* **10**, 1716–1722 (1993).

- <sup>30</sup>L. Yu and Z.-Z. Yang, *J. Chem. Phys.* **132**, 174109 (2010).
- <sup>31</sup>P.-J. Hsu, K.-L. Ho, S.-H. Lin, and J.-L. Kuo, *Phys. Chem. Chem. Phys.* **19**, 544–556 (2017).
- <sup>32</sup>M. J. Frisch, G. W. Trucks, H. B. Schlegel, G. E. Scuseria, M. A. Robb, J. R. Cheeseman, G. Scalmani, V. Barone, B. Mennucci, G. A. Petersson, H. Nakatsuji, M. Caricato, X. Li, H. P. Hratchian, A. F. Izmaylov, J. Bloino, G. Zheng, J. L. Sonnenberg, M. Hada, M. Ehara, K. Toyota, R. Fukuda, J. Hasegawa, M. Ishida, T. Nakajima, Y. Honda, O. Kitao, H. Nakai, T. Vreven, J. A. Montgomery, Jr., J. E. Peralta, F. Ogliaro, M. J. Bearpark, J. Heyd, E. N. Brothers, K. N. Kudin, V. N. Staroverov, R. Kobayashi, J. Normand, K. Raghavachari, A. P. Rendell, J. C. Burant, S. S. Iyengar, J. Tomasi, M. Cossi, N. Rega, N. J. Millam, M. Klene, J. E. Knox, J. B. Cross, V. Bakken, C. Adamo, J. Jaramillo, R. Gomperts, R. E. Stratmann, O. Yazyev, A. J. Austin, R. Cammi, C. Pomelli, J. W. Ochterski, R. L. Martin, K. Morokuma, V. G. Zakrzewski, G. A. Voth, P. Salvador, J. J. Dannenberg, S. Dapprich, A. D. Daniels, O. Farkas, J. B. Foresman, J. V. Ortiz, J. Cioslowski, and D. J. Fox, *GAUSSIAN 13*, Revision E.01, Gaussian, Inc., Wallingford, CT, USA, 2013.
- <sup>33</sup>V. Barone, *J. Chem. Phys.* **122**, 014108 (2005).
- <sup>34</sup>W. H. Miller, R. Hernandez, N. C. Handy, D. Jayatilaka, and A. Willetts, *Chem. Phys. Lett.* **172**, 62–68 (1990).
- <sup>35</sup>E. P. L. Hunter and S. G. Lias, *J. Phys. Chem. Ref. Data* **27**, 413–656 (1998).
- <sup>36</sup>Y. Matsuda, M. Mori, M. Hachiya, A. Fujii, and N. Mikami, *Chem. Phys. Lett.* **422**, 378–381 (2006).
- <sup>37</sup>H. L. Han, C. Camacho, H. A. Witek, and Y. P. Lee, *J. Chem. Phys.* **134**, 144309 (2011).
- <sup>38</sup>L. Jiang, T. Wende, R. Bergmann, G. Meijer, and K. R. Asmis, *J. Am. Chem. Soc.* **132**, 7398–7404 (2010).
- <sup>39</sup>T. Shimanouchi, *J. Phys. Chem. Ref. Data* **6**, 993–1102 (1977).